Testing the Concept of Drift Shadow with X-Ray Absorption Imaging

Susan J. Altman, Aleeca Forsberg, William Peplinski, and Clifford K. Ho

Sandia National Laboratories: Geohydrology Department, P.O. Box 5800, Albuquerque, New Mexico, 87185-0735
sjaltma@sandia.gov

Abstract *– X-ray absorption imaging experiments and measurements of inflow and outflow distribution provide quantitative and visual evidence for capillary diversion around a drift and a drift-shadow effect. Test cells were constructed from volcanic tuff with either in-plane (one fracture parallel to the face of the test cell) or multi-fracture (with a grid of fractures perpendicular to the test cell) systems. Tracer solutions were dripped in the fractures at ports along the top of the test cell. Discharge along the bottom boundary and in the drift was monitored. Variables included flow rate and fracture aperture. X-ray absorption imaging allowed for visualization of flow paths through the system. Evidence for capillary diversion and drift shadow include: 1) very small (< 1% of inflow in most cases) measured discharge into the drift, 2) discharge less than expected under the drift and discharge greater than expected just beyond the drift, and 3) visualization of the tracer-solution flow path from above the drift, around the drift, and shedding beyond the drift. However, tracer was also observed in a natural fracture under the drift in one system. It is unclear whether these high concentrations are due to diversion around the drift and back under the drift or capillary spreading along the bottom boundary of the test cell. Future experiments will focus on using samples collected directly from Yucca Mountain and minimizing the capillary barrier effects along the lower boundary of the test cells. The implementation of the drift shadow effect, as supported by these experiments, could impact performance of the proposed Yucca Mountain repository.*

I. INTRODUCTION

The analytical model of Philip et al. [1] predicts flow diversion around drifts due to the presence of a capillary barrier resulting in a dry area beneath the drift called the drift shadow. According to the analytical model, the amount of drift diversion and outflow location are controlled by the drift diameter, capillary pressure and fracture aperture. In contrast to Philip et al.'s [1] model, the current Yucca Mountain performance assessment models conservatively assume that the percolation flux directly under the drifts is the same as the flux away from the drifts. In other words, the Yucca Mountain performance assessment does not take credit for the drift-shadow effect. Through X-ray absorption laboratory experiments, we test the concept of the drift shadow. These studies provide quantitative and visual evidence that only a fraction of the total percolation flux is available for transporting radionuclides immediately beneath the repository.

II. METHODS

X-ray absorption imaging [2, 3] is an experimental technique that allows for the visualization and quantification of transport through geological media. X-ray absorption imaging along with mass-balance measurements of tracer solution flowing into and out of the system provide two lines of evidence of where the tracer solution is flowing through the sample.

II.A. Test Cell Description

Test cells with sample dimensions 10 cm × 15 cm × 2.5 cm have been constructed from non-Q (a Q designation means that the acquisition and use of the sample is controlled and traceable) Topapah Spring Tuff samples, a volcanic tuff with pumice fragments. An approximately 8-cm-diameter "drift" was cored from the cells. Symmetry is assumed for these experiments, thus the drifts consist of a semi-circle. Test cells were prepared with different fracture configurations and apertures (Fig. 1). One fracture configuration has a grid of fractures perpendicular to the face of the flow cell (Figure 1a, multi-fracture system). The second configuration has one fracture parallel to the face of the flow cell (Fig. 1b, in-plane fracture system). Fracture aperture is controlled by placing wires of known diameter of either 100 μm, 250 μm, or 500 μm in the fractures. Wire spaces were 1.5 cm long and placed at the top and bottom of the in-plane fracture systems. They were evenly spaced between the injection and sampling ports so to minimize their impact on flow. After placement of the wires in the fractures, the cells were encased by aluminum bars on the sides and epoxy on the faces. The

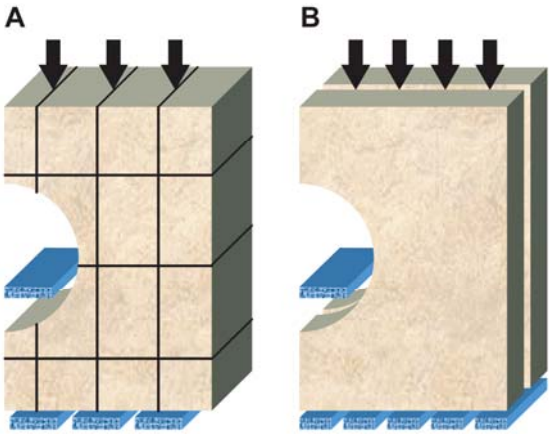

Fig. 1. Schematic of multi-fracture (A) and in-plane fracture (B) configurations.

frame and epoxy provide rigidity to the test cell, minimize X-ray scatter around the edges of the sample, and provide no-flux boundaries where needed. The aluminum bars were constructed such that needles could be placed along the top boundary to introduce the tracer. Sampling ports were added within the drift and along the bottom boundaries. These ports could be closed when samples were not being collected. This paper describes the experiments performed with the in-plane fracture test cells.

II.B. Experiment Description

To date, a total of 17 experiments have been run (Table 1). Prior to starting an experiment, the in-plane test cells were saturated with water. At the start of the experiment, a 10% by weight potassium iodide (KI) tracer solution was dripped at a controlled flow rate through four ports at the top of the test cells. Transport through the cell was measured by collecting and weighing sponges both in the drift and at collection ports at the bottom of the flow cell (Fig. 1). The multi-fracture tests were run similarly, except that in the first test the cells were initially saturated with the KI solution and clean water was used as the tracer. Potassium iodide was chosen as the tracer because it is geochemically conservative and has favorable X-ray absorption characteristics.

Sponges were collected from the ports approximately every 10 – 15 minutes. For slower flow rates, more time was allowed between sponge collection. Sponges were weighed dry before insertion into the test cell and after removal from the test cell. Thus, the difference in mass was an indication of the mass discharged from each port. Mass in the system was estimated by multiplying flow rate by the number of ports, the density of the solution and the duration of the test. Mass out was calculated by adding the cumulative mass discharge for each port based on the sponge weighing. Thus, the mass balance errors were calculated as:

TABLE 1: Experiment Summary

Flow Rate (ml/min)	Fracture Aperture (μm)	Test Duration (min)	Mass Balance Error (%)	Cum. Mass into Drift (%)
In-Plane Fracture Tests				
0.01	100	485	10	0.9
0.01	250	485	-4.5	0.0
0.01	500	360	4.2	1.9
0.05	100	320	11	0.6
0.05	250	320	10	1.2
0.09	100	126	7.9	0.2
0.09	250	126	1.6	0.3
0.10	250	300	10.4	0.2
0.12	100	132	9.9	0.9
0.13	250	132	9.7	0.3
0.24	250	213	7.2	0.10
0.23	500	213	11.2	0.14
Multi-Fracture Tests				
0.01	100	421	-10.0	3.0
0.1	100	141	3.8	0.8
0.1	250	141	3.4	0.3
0.1	250	146	11.4	0.5
0.1	100	300	8.7	0.5

$$Error = \frac{Mass_{In} - Mass_{Out}}{Mass_{In}} \quad (1)$$

For the tests that lasted over a day, mass balances were only calculated for approximately 8 hours.

The distribution of outflow is presented as bar charts showing the cumulative normalized fraction of inflow from each port. In this case, the outflow is normalized by the fraction of flow that would be expected if flow was vertical through the system. As the ports are equally spaced, it is expected one fifth of the inflow will discharge through each port (for the in-plane configuration). Thus the cumulative fraction of inflow is normalized by 0.20.

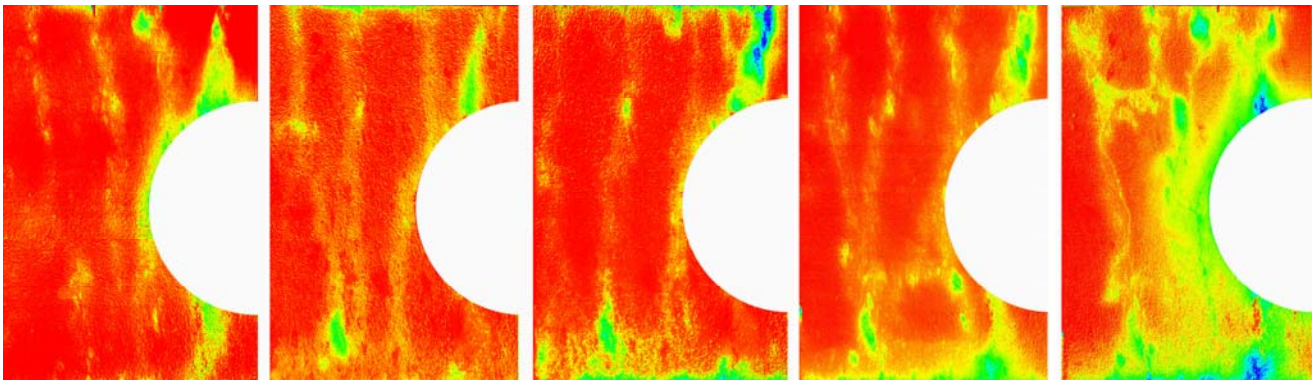

Fig. 2. X-ray absorption images of the 250-µm aperture in-plane test cell taken 5 hours after start of experiments run at noted flow rates. Numbers below the flow rates refer to the order in which the experiments were run. Yellow going to green and then blue indicates increasing tracer concentrations.

Test cells were used for more than one experiment. Between experiments the test cells were soaked in clean water to allow for the KI to diffuse out of the test cell. The specific conductivity of the solution in which the cells soaked was measured periodically. When the specific conductivity was high, the water was changed. Soaking occurred until the specific conductivity of the soaking water did not increase above its background. Clean water was also dripped through the system for at least 15 hours prior to introduction of the tracer.

II.C. Image Analysis

X-ray images were collected prior to the start of the experiment and at different times during the experiment for the purpose of visualizing flow paths through the system. Here we present images taken 5 hours after the start of the introduction of the tracer. The film was digitized using a Microtek ScanMaker 9800XL scanner with the TMA 1600 attachment to allow transmitted light through the X-ray. Each X-ray film was scanned 55 times at a resolution of 300 dots per inch (dpi). These 55 images were then aligned with each other and the grey-scale values at each pixel averaged to reduce the noise due to the scanner. Grey-scale values ranged from 0 to 65,535. Grey-scale values are a function of the transmission of X-rays through the sample. A more dense area will have less X-rays transmitted than a less dense area.

By subtracting the digitized image taken prior to the start of the experiment from the digitized images taken during the experiment, the X-ray absorption due to the geological media was removed, and the tracer solution pathways in the geological samples become visible. Prior to subtraction, the two images need to be aligned with each other to reduce noise. It should be noted that at this stage of the research, the images are only being used for qualitative inspection of movement of the water through our test cells. Thus, in some cases, the alignment of the images was not rigorous. However, we are in the process of improving our alignment software to make the alignment process more precise.

III. RESULTS AND DISCUSSION

There is clear evidence for capillary diversion around the drift from both the X-ray absorption images (Figs. 2 and 3) and the distribution of outflow data (Table 1, Fig. 4). The X-ray images show accumulation of tracer above the drift and tracer flow paths going around the drift. In addition, in all but 2 of the tests, less than 1% of the inflow mass was discharged into the drift (Table 1).

There is also evidence for the drift shadow effect. Discharge from the port directly under the drift (port 1) is

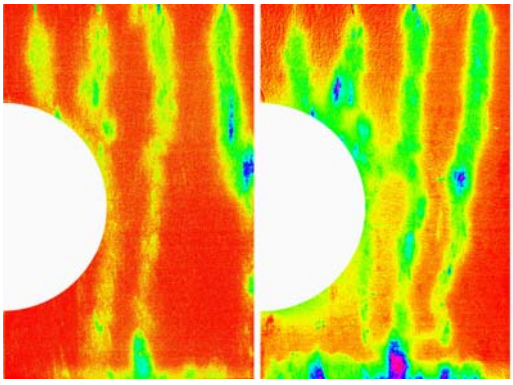

Fig. 3. X-ray absorption images of the 500-µm aperture in-plane test cell taken 5 hours after start of experiments run at noted flow rates. Numbers below the flow rates refer to the order in which the experiments were run. Yellow going to green and then blue indicates increasing tracer concentrations.

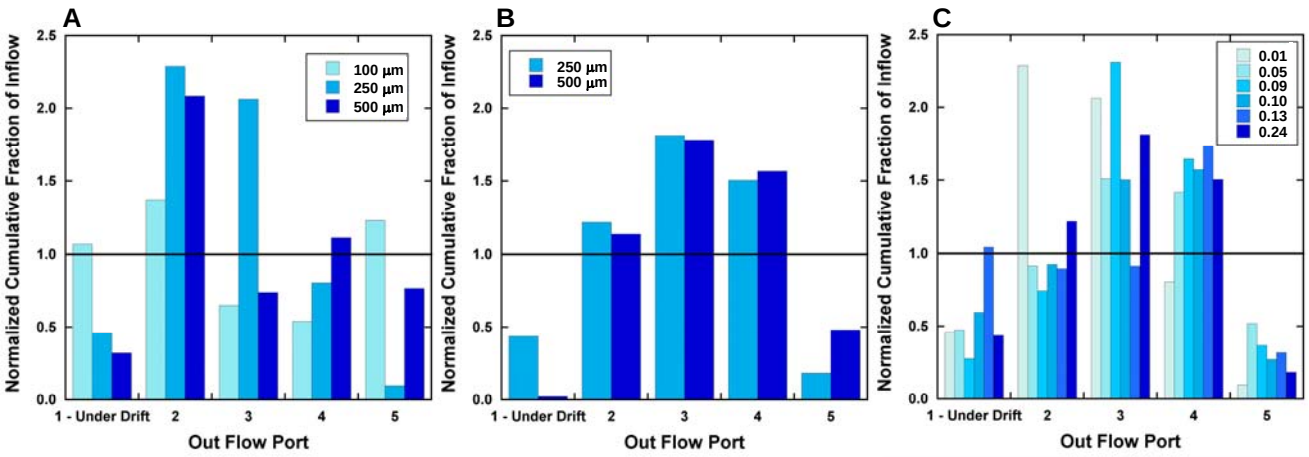

Fig. 4. Fraction of inflow discharging through outflow ports for 0.01 ml/min flow rate (A) and 0.23 ml/min flow rate (B) as a function of fracture aperture and 250-µm-aperture fracture as a function of flow rate (ml/min) (C). Fractions are normalized such that if the inflow was discharged uniformly the normalized discharge would be 1.

almost always less than would be expected if flow were vertical (Fig. 4). Furthermore, for the in-plane fracture systems with 250-µm apertures discharge was greater than expected at the ports at the edge of the drift (ports 3 and/or 4, Fig. 4C). For two tests, the discharge was more than twice what was expected in port 3 than if flow was uniformly vertical. X-ray absorption imaging provided strong visual evidence of the drift-shadow effect. In many of the tests a flow path was observed starting from the injection port above the drift, and discharging through port 3 (Figs. 2 and 3). It should be noted that the 100-µm-aperture in-plane system had too small an aperture to contain enough KI such that the flow paths are readily visible.

Images obtained from the X-ray absorption imaging also show that flow paths changed from test to test (Fig. 2 and 3). This is most evident for the path starting from the port farthest from the drift on the 250-µm-aperture system (Fig. 2). In one case (0.09 ml/min) the flow is almost vertical. For the tests run at 0.01, 0.05, and 0.13 ml/min the flow tends to go towards the drift and eventually merges with the flow path coming from the injection port directly to the right near the bottom of the test cell. For the test run at 0.24 ml/min the flow paths from these two injection ports intersect higher in the test cell. There are two possible explanations for evolution of the flow paths. It is possible that the flow path is dependent on the flow rate. Another explanation is that changes in surface chemistry over time affected the permeability of the heterogeneous flow system. These permeability changes in turn alter flow paths. As the change in flow paths seems more related to the order of the tests than the flow rate, we believe the latter explanation is more probable.

The X-ray imaging also shows that a capillary fringe is developing along the bottom of the test cell (Figs. 2 and 3). The size of the fringe increases with increasing flow rates. While our sponges generally abutted the bottom boundary, capillary pressure of the sponge might not have been great enough to draw the solutions out from the in-plane fracture. This capillary fringe could be responsible, in-part, for lateral spreading of tracer along the bottom boundary of the test cells.

Finally, the X-ray images show that natural heterogeneities have some control on the flow paths of the system. One of the major differences between the 250-µm and the 500-µm-aperture in-plane fracture systems is that in the 250-µm system a fracture developed in a highly porous pumice portion of the matrix during sample preparation. This fracture is located directly under the drift. The greater tracer concentration in this fracture is evident in many of the tests, especially the ones run at higher flow rates (Fig. 2). For the 500-µm-aperture in-plane fracture system, a flow path from the bottom of the drift to the bottom of the test cell is not visible, indicating the importance of the fracture in the 250-µm system. It is unclear whether the tracer is distributed to this fracture through flow around the drift or through the lateral spreading along the capillary fringe on the lower boundary.

With one exception, trends in discharge as a function of fracture aperture or flow rate are not readily apparent (Fig. 4). Changes in flow path as a function of flow rate or test order could explain why such trends are not observed. The one observed trend is that discharge under the drift appears to decrease as fracture aperture increases at both flow rates of 0.01 ml/min and 0.24 ml/min (Fig. 4A and B). This trend is expected because with lower flow rates capillary forces are expected to dominate more than gravity forces, thus, spreading within the in-plane fracture is more likely. The capillary forces will allow for

the tracer to be diverted back under the drift after flowing around the drift, as opposed to shedding vertically off the edge of the drift.

IV. CONCLUSIONS

The experiments provide evidence for a drift shadow. This is seen by discharge less than expected under the drift and discharge greater than expected just beyond the drift then if flow was uniformly vertical. X-ray absorption imaging also shows a tracer-solution flow path from above the drift being diverted around the drift and shedding beyond the drift. However, we also observe high tracer concentrations in the natural fracture under the drift in the 250-μm-facture aperture system. It is unclear whether these high concentrations are due to diversion around the drift and back under the drift or capillary spreading along the bottom boundary of the test cell.

There is strong evidence of capillary diversion around the top of the drift. The X-ray absorption imaging shows flow paths over the drift being diverted around the drift in the 250-mm aperture cell. In addition, measured discharge into the drift was very small.

Future experiments will focus on using quality (Q) samples collected directly from Yucca Mountain. Experimental design will be improved to minimize the capillary barrier effects along the lower boundary of the test cells.

These studies provide quantitative and visual evidence that only a fraction of the total percolation flux is available for transporting radionuclides immediately beneath the repository. This evidence is important information for performance assessment and, if implemented, could lead to improved natural barrier performance in future calculations. However, it is still necessary to quantify the amount and variability of flux below the drift before making recommendations for performance assessment calculations.

ACKNOWLEDGMENTS

We thank Fotini Walton and Amanda Valencia for their assistance in running the experiments. This project was funded by the Department of Energy, OCRWM, Office of Science and Technology and International. Sandia is a multiprogram laboratory operated by Sandia Corporation, a Lockheed Martin Company for the United States Department of Energy's National Nuclear Security Administration under contract DE-AC04-94AL85000.

REFERENCES

[1] J. R. PHILIP, J. H. KNIGHT, and R. T. WAECHTER, "Unsaturated seepage and subterranean holes - conspectus, and exclusion problem for circular cylindrical cavities," *Water Resources Research*, **25**(1), 16-28 (1989).

[2] V. C. TIDWELL, V.C., L. C. MEIGS, T. CHRISTIAN-FREAR, and C. M. BONEY, "Effects of spatially heterogeneous porosity on matrix diffusion as investigated by X-ray absorption imaging," Journal of Contaminant Hydrology, **42**, 285-302 (2000).

[3] S. J. ALTMAN, M. UCHIDA, V. C. TIDWELL, C. M. BONEY, and B. P. CHAMBERS, "Use of X-ray Absorption Imaging to Examine Heterogeneous Diffusion in Fractured Crystalline Rocks," Journal of Contaminant Hydrology, **69**, 1-26 (2004).